AIAA JOURNAL
Vol. 35, No. 5, May 1997

Incremental Potential Flow Based Membrane Wing Element

Rick Smith* and Wei Shyy†
University of Florida, Gainesville, Florida 32607

A new quadrilateral membrane wing element is presented that combines an incremental formulation of the elastic membrane problem with a vortex lattice formulation of the thin wing aerodynamic problem. The incremental formulation leads to an explicit/implicit velocity-stepping algorithm for solving the coupled aeroelastostatic membrane wing problem. The Stein–Hedgepeth wrinkle model is adopted as the constitutive relation for the membrane, which may develop slack or wrinkled regions. The element is shown to satisfy two limiting cases of the aeroelastic problem for which there are well-known analytic solutions. The algorithm is applied to two moderate aspect ratio membrane wing configurations with the second configuration being a model of a marine sail.

I. Introduction

IT is fair to say that flexible membrane wings have received only a small fraction of the technological attention that has been given to rigid wings and airfoils since the early days of flight. This is somewhat surprising since many flying machines from the Wright Flyer to the Gossamer Albatross have featured, either intentionally or by default, lifting surfaces that significantly deformed under normal aerodynamic loading and in turn had their aerodynamic properties altered by the material deformation. With membrane wings, e.g., marine sails, Rogallo wings, and self-inflating parawings, the configuration of the wing is dictated by an equilibrium between the tension field in the membrane and the aerodynamic stresses. By judicious choice of materials, pretension, and unstrained configuration, an aerodynamically effective equilibrium configuration can often be achieved for the lifting surface. This judicious choice has historically been the responsibility, and indeed the art, of the sailmaker and wing designer. Only over the last decade or so have computational methods begun to supplement what has traditionally been an intuitive and empirical approach to membrane wing design.

Here we present a computational algorithm for analyzing membrane wing mechanics with the simplifying assumption that the fluid mechanics can be meaningfully approximated by a potential flow description. This assumption has been made by almost all membrane wing theories to date for general three-dimensional geometries such as those of Jackson[1] and Jackson and Christie.[2] The present work follows closely in spirit the work of Jackson and Christie[2] but it differs significantly from their seminal work in several ways. First, a bilinear quadrilateral plane stress element is adopted in the elastic model, which readily accommodates the conventional arrangement of vortex filaments and control points in the aerodynamic model. Second, an incremental continuum-based formulation of the elastic membrane problem is taken as the basis for a velocity-stepping procedure for the solution of the aeroelastic problem. This formulation leads to an explicit/implicit algorithm, which offers considerable flexibility in solving a variety of membrane wing problems. Finally, a wrinkle model proposed by Miller and Hedgepeth[3] is adopted as the constitutive relationship between stress and strain in the membrane, which may develop slack or wrinkled regions.

Several works have appeared in the literature over the years that have considered various idealizations of the general three-dimensional membrane wing problem. A two-dimensional theory was combined in a stripwise fashion with lifting line theory by Neilsen,[4] Sneyd,[5] and Ormiston.[6] Murai and Maruyama[7] developed a model for a rectangular planform wing assuming the tension in the chordwise direction to be zero. Holla et al.[8] also investigated a rectangular membrane wing with fixed edges assuming a state of uniform biaxial tension to exist in the membrane. Kroo[9] developed a numerical method for arbitrary planforms and edge conditions, which was based on a strain energy formulation of the elastic problem and a vortex lattice treatment of the potential flow problem. Kroo[9] used this model to investigate the stability of hang gliders. In a related topic, the classical two-dimensional inextensible membrane airfoil problem[10] has been investigated computationally by Smith and Shyy.[11,12] A comprehensive review of two-dimensional and finite span membrane wing theories proposed before 1987 is given by Newman.[13]

The numerical model developed by Jackson[1] and Jackson and Christie[2] is probably the most general three-dimensional model presented to date and has been widely applied to the aeroelastic analysis of marine sails. This model combines a triangular vortex lattice treatment of the lifting potential flow problem with a constant strain finite element formulation of the elastic membrane problem. Results for rectangular and triangular planform membrane wings with several different edge boundary conditions and elastic parameters were presented.

II. Theoretical Model

A. Elastic Membrane Problem

The principle of virtual work is used to formulate the finite element matrices for a bilinear quadrilateral, plane stress membrane element. The total Lagrangian formulation is used in deriving the element, which may undergo large displacements and rotations but is assumed to undergo only small strains. The formulation and nomenclature follows the work of Bathe.[14] Index notation with the summation convention is used throughout and a comma implies partial differentiation with respect to the indicated independent variable.

Figure 1 shows a material volume undergoing large deformation from a natural unstrained state at time $t = 0$ through an intermediate state at time t to a final deformed configuration at time $t + \Delta t$. In the aeroelastostatic formulation developed here, the timelike coordinate t is used only as a convenient parameter for describing the loading and deformation state and does not imply the existence of a dynamic process. The statement of equilibrium for the continuum at configuration $t + \Delta t$ is given by the principle of virtual work as

$$\int_{0_V} {}^{t+\Delta t}S_{ij}\,\delta\left({}^{t+\Delta t}\varepsilon_{ij}\right)\,{}^{0}\mathrm{d}V = {}^{t+\Delta t}R \tag{1}$$

where S_{ij} is the second Piola–Kirkoff stress tensor, ε_{ij} is the Green's strain tensor, δ is an admissible variation, and R is the virtual work performed by external forces on the material volume at time $t + \Delta t$.

The incremental decomposition[14] of the stresses, strains, displacements, and material coordinates are given by

$${}^{t+\Delta t}\varepsilon_{ij} = {}^{t}\varepsilon_{ij} + \varepsilon_{ij} \tag{2a}$$

$${}^{t+\Delta t}S_{ij} = {}^{t}S_{ij} + S_{ij} \tag{2b}$$

$${}^{t+\Delta t}u_i = {}^{t}u_i + u_i \tag{2c}$$

$${}^{t+\Delta t}x_i = {}^{t}x_i + u_i \tag{2d}$$

Received July 24, 1996; revision received Feb. 6, 1997; accepted for publication Feb. 10, 1997.

*Postdoctoral Research Fellow, Department of Aerospace Engineering, Mechanics, and Engineering Science.

†Professor and Chairman, Department of Aerospace Engineering, Mechanics, and Engineering Science. Associate Fellow AIAA.

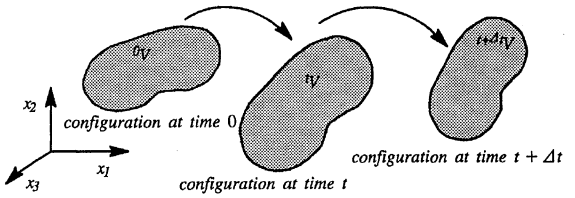

Fig. 1 Deformation trajectory of material volume ${}^0V$.

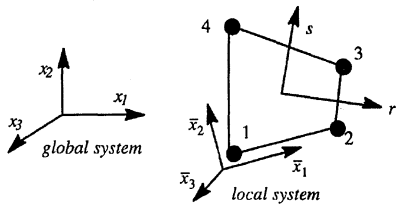

Fig. 2 Plane stress quadrilateral element with local and global coordinate systems.

where ε_{ij}, S_{ij}, and u_i are increments in strain, stress, and displacement, respectively. Using these decompositions in Eq. (1), along with the approximations

$$S_{ij} \approx C_{ijrs} e_{rs} \tag{3a}$$

$$\delta\varepsilon_{ij} \approx \delta e_{ij} \tag{3b}$$

gives the following linearized incremental equation of equilibrium:

$$\int_{0V} C_{ijrs} e_{rs}\, \delta e_{ij}\, {}^0\mathrm{d}V + \int_{0V} {}^tS_{ij}\, \delta\eta_{ij}\, {}^0\mathrm{d}V = {}^{t+\Delta t}R - \int_{0V} {}^tS_{ij}\, \delta e_{ij}\, {}^0\mathrm{d}V \tag{4}$$

where C_{ijrs} is the material property tensor and e_{ij} and η_{ij} are the linear and nonlinear components, respectively, of the incremental strain tensor given by

$$e_{ij} = \tfrac{1}{2}\left(u_{i,j} + u_{j,i} + {}^tu_{k,i}u_{k,j} + u_{k,i}{}^tu_{k,j}\right) \tag{5a}$$

$$\eta_{ij} = \tfrac{1}{2}\left(u_{k,i}u_{k,j}\right) \tag{5b}$$

After introducing bilinear isoparameteric interpolations for a four-noded quadrilateral element, as shown in Fig. 2, the linearized incremental equation of equilibrium can be written in discrete form as

$$\left([{}^tK_L] + [{}^tK_{\mathrm{NL}}]\right)[U]^{(i)} = [{}^{t+\Delta t}R]^{(i-1)} - [{}^{t+\Delta t}F]^{(i-1)} \tag{6}$$

where K_L and K_{NL} are the linear and nonlinear element stiffness matrices, respectively, U is the vector of nodal incremental displacements, and R and F are the nodal load and force vectors, respectively. Details of the element matrices are given in the Appendix. Equation (6) can be viewed as a modified Newton–Raphson formula for the solution of the nodal displacements with the right-hand superscript indicating the iteration number.

As mentioned, the timelike coordinate t is simply a parameter that is used to describe the deformation path when the structural load is applied in increments or steps: hence, the customary term load stepping.[14] Here, the structural load is the aerodynamic pressure, which varies with the square of the freestream velocity. Consequently, in the aeroelastic problem, the aerodynamic load is applied by incrementally increasing the freestream velocity in steps to some final desired value: hence, the term velocity stepping.

Inasmuch as the element matrices are evaluated in a local element coordinate system they must be transformed to the global coordinate system prior to assembly. These transformations are accomplished using the conventional first- and second-order tensor transformations given by

$$[K] = [T][\bar{K}][T]^T \tag{7a}$$

$$[F] = [T][\bar{F}] \tag{7b}$$

$$[R] = [T][\bar{R}] \tag{7c}$$

where $[T]$ is the matrix of direction cosines relating the global system to the local system.[15] After transformation, the system of global equilibrium equations is assembled using the direct stiffness method. The nodal displacement increment residual for the assembled system is defined as

$$R_U = \sum_{\text{all DOF}} \left|\frac{U}{b}\right| \tag{8}$$

where b is the membrane span and the sum is over all unconstrained degrees of freedom.

B. Wrinkle Model

The constitutive model for partially wrinkled membranes originally proposed by Stein and Hedgepeth[16] and later refined by Miller and Hedgepeth[3] and Miller et al.[17] is adopted here. The Stein–Hedgepeth model is an approximate theory that attempts only to identify the stress state and average wrinkle strain within the tension field and does not address the detailed shape of the wrinkled surface.

The need for considering the existence of wrinkling in the membrane stems primarily from the fact that under certain conditions of aerodynamic loading, elastic boundary conditions, and initial geometry, wrinkled or slack regions may develop over portions of the membrane surface. Under these conditions a tension field exists, and the isotropic plane stress constitutive law no longer applies. Consequently, a modified constitutive law is required in these regions. A secondary, perhaps more subtle reason for including a wrinkle model in the present formulation, is that during the solution of the aeroelastic problem the tangent stiffness matrix of the discrete system is assembled prior to applying the next freestream velocity increment. If compressive stresses are allowed to develop at any point along the deformation trajectory the conditioning of the tangent stiffness matrix will deteriorate. If the compressive stresses are widespread the tangent stiffness matrix will become algorithmically singular and the solution procedure will fail. The Stein–Hedgepeth constitutive model preempts the development of compressive principal stresses in the membrane whenever wrinkling conditions are encountered and maintains the positive definiteness of the tangent stiffness matrix.

In a wrinkled region the Stein–Hedgepeth model assumes a uniaxial stress state to exist in the membrane in the principal strain coordinate directions. For a Hookean material, the postwrinkling tension field stresses are given by

$$\sigma_1 = E\varepsilon_1 \qquad \text{and} \qquad \sigma_2 = 0 \tag{9a}$$

where σ_1 and σ_2 are the ordered principal stresses, ε_1 is the largest principal strain, and E is Young's modulus.

Following the nomenclature of Miller et al.,[17] three constitutive relationship are possible for a partially wrinkled membrane made of an isotropic linearly elastic material. These constitutive relationship are

$$[C] = \begin{cases} C_S; & \varepsilon_1 \le 0 \\ C_W; & \varepsilon_1 > 0 \quad \text{and} \quad \varepsilon_2 < -\nu\varepsilon_1 \\ C_T; & \text{otherwise} \end{cases} \tag{9b}$$

for slack, wrinkled, and taut regions, respectively, where the constitutive property matrices are given by

$$[C_S] = [0] \tag{9c}$$

$$[C_W] = \begin{bmatrix} (E/2)(1+P) & 0 & EQ/4 \\ 0 & (E/2)(1-P) & EQ/4 \\ EQ/4 & EQ/4 & E/4 \end{bmatrix} \tag{9d}$$

$$[C_T] = \left(\frac{E}{1-\nu^2}\right)\begin{bmatrix} 1 & \nu & 0 \\ \nu & 1 & 0 \\ 0 & 0 & (1-\nu)/2 \end{bmatrix} \tag{9e}$$

where ν is Poisson's ratio and P and Q are defined as

$$P = \frac{\varepsilon_{11} - \varepsilon_{22}}{\varepsilon_1 - \varepsilon_2} \qquad \text{and} \qquad Q = \frac{2\varepsilon_{12}}{\varepsilon_1 - \varepsilon_2} \tag{9f}$$

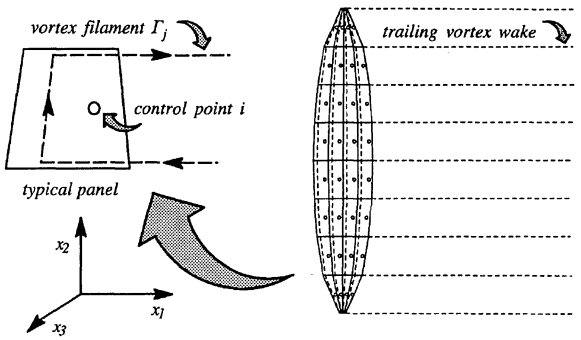

Fig. 3 Discretization of an elliptical planform thin wing into quadrilateral panels.

The constitutive property matrix that applies under taut conditions can be recognized as the isotropic plane stress linear elastic constitutive law.

C. Aerodynamic Problem

The fundamental assumption concerning the flowfield around the wing is that it is irrotational, and consequently the velocity field may be derived from a scalar potential. Implicit in this assumption is that the flow is inviscid, incompressible, and free of vorticity far upstream. The validity of this assumption has been investigated for membrane airfoils by Smith and Shyy.[12] The use of a lattice of vortex filaments to model the lifting potential flow around thin wings has its historical origin and justification in work by James.[18] A description of the method in its modern form for wings of finite span may be found in Ref. 19.

Figure 3 shows a thin wing that has been discretized into a number of quadrilateral panels. A typical panel is composed of a horseshoe-shaped vortex filament of strength Γ_j and a control point where the flow tangency condition is enforced. By modeling the wing as an assemblage of vortex singularity segments of unknown strength and enforcing the zero normal velocity condition at each control point the following set of linear algebraic equations may be formed:

$$A_{ij}\Gamma_j = (-\boldsymbol{v}_\infty \cdot \boldsymbol{n})_i \tag{10a}$$

where A_{ij} is the matrix of vortex influence coefficients, $\boldsymbol{v}_\infty$ is the freestream velocity vector, and $\boldsymbol{n}$ is the panel unit normal vector. If the vortex filaments and control points are located at the local quarter and three-quarter chord points of the panel, respectively, the Kutta condition is implicitly satisfied, and no additional boundary condition is needed at the trailing edge.[18,19] Although no left-hand superscript is given in Eq. (10a) indicating the time index of the configuration or velocity step, it should be clear that the aerodynamic pressures are to be evaluated at the current configuration and velocity step at time $t + \Delta t$.

Once the circulation strength for each panel has been determined from Eq. (10a) the force vector $\mathcal{F}$ acting on the element is given by the generalized Kutta–Joukowski theorem (see Ref. 19) as

$$\mathcal{F} = \varrho l(\boldsymbol{v} \times \boldsymbol{\Gamma}) \tag{10b}$$

where ϱ is the fluid density, l is the length of the bound segment of the vortex filament, $\boldsymbol{v}$ is the total velocity vector at the control point, and $\boldsymbol{\Gamma}$ is the circulation vector associated with the bound vortex filament. The net pressure difference acting on the element, Δp, is then simply given by the magnitude of $\mathcal{F}$ divided by the panel area. The total lift and drag on the wing is determined by summing up the force contributions from each bound vortex filament over the entire wing using a far-field analysis, which correctly accounts for the downwash and induced drag on the wing.[19]

D. Nondimensionalization

By considering two limiting cases, the case when membrane tension is dominated by elastic strain and, alternately, when tension is dominated by prestrain, two dimensionless parameters emerge that characterize the aeroelastostatic membrane wing problem. These parameters are an aeroelastic parameter Π_1 and a prestrain parameter Π_2. These parameters are defined as

$$\Pi_1 = (Ed/q_\infty b)^{\frac{1}{3}} \quad \text{and} \quad \Pi_2 = \left({}^0\varepsilon Ed/q_\infty b\right) \tag{11}$$

where d is the membrane thickness, b is the wing span, ${}^0\varepsilon$ is the membrane prestrain, and q_∞ is the freestream stagnation pressure equal to $\frac{1}{2}\varrho v_\infty^2$. The use of the cube root in the definition of Π_1 in Eq. (11) is suggested by an analytic solution for a pressure loaded membrane given by Seide.[20] The aeroelastic parameter Π_1 is identical to the aeroelastic number proposed by Jackson and Christie[2] with the exception of the cube root. Here membrane wings without pretension are investigated. Consequently, Π_2 is zero and the set of dimensionless parameters defining the aeroelastostatic problem is reduced to Π_1 and α for a membrane wing with specified material, geometry, and boundary conditions.

E. Aeroelastic Problem

The development of a computational procedure for the analysis of flexible membrane wings may be sensibly divided into two parts: the development of a viable membrane wing element and the development of a solution strategy for the coupled aeroelastic problem. In developing such a procedure, many options are available in terms of both the aeroelastic element technology and the overall solution strategy. Of course, the discretizations chosen for the elastic and aerodynamic problems were such that a hybrid aeroelastic element could be easily formed by combining the plane stress quadrilateral element with the quadrilateral vortex panel described earlier.

Recalling the load-stepping procedure first introduced for solving the elastic problem, it is natural to extend this methodology to a velocity-stepping procedure for the solution of the aeroelastic problem. Furthermore, because a number of iterations are required at each velocity step in the elastic problem in order to satisfy equilibrium, it is again natural to evaluate the aerodynamic pressures based on the updated wing configuration during each iteration. This procedure guarantees that the wing configuration and the aerodynamic loading are in equilibrium at the end of each velocity step. However, iterating at each velocity step in order to achieve aeroelastic equilibrium is quite expensive because the computation of the aerodynamic surface pressures involves the solution of a large system of linear equations with a full nonsymmetric coefficient matrix. Consequently, the CPU time required to solve the aerodynamic problem increases much more rapidly with problem size than the CPU time required to solve the elastic problem. This situation is a direct result of the bandedness of the assembled stiffness matrix and the fullness of the assembled aerodynamic coefficient matrix.

III. Results and Discussion

A. Basic Test Cases

Before applying the method to a membrane wing problem, two limiting cases of the aeroelastic problem are investigated and the results are compared with well-known analytic solutions. The two limiting cases are the deformation of a square, initially flat, edge constrained, elastic membrane subjected to uniform pressure load and the lift curve slope of a rigid, elliptical planform flat plate of moderate aspect ratio.

Figure 4a shows the computed transverse midpoint deflection of the membrane subjected to a uniform pressure load. All displacement degrees of freedom (${}^t u_i$, $i = 1, 2, 3$) along the membrane perimeter were set to zero for this calculation. Results are shown for several different values of the dimensionless stiffness parameter Π_1, where uniform pressure has been substituted for the stagnation pressure in the definition of Π_1. The midpoint deflection u_3 is nondimensionalized in the figure by the membrane edge dimension c and Poisson's ratio is taken to be 0.3. The agreement between the computed solution and the analytic solution[20] is seen to be quite good.

Note that for this configuration and boundary condition set no Gauss points reported a wrinkled or slack condition, and consequently the isotropic relationship [Eq. (9e)] was the only active constitutive law. However, this situation is the exception rather than the norm for general membrane configurations. As will be seen in the following examples, wrinkling often prevails over large portions of the membrane and the alternate nonisotropic wrinkled constitutive law [Eq. (9d)] is predominant. This has been observed to be particularly true for triangular planform configurations.[1]

Because the membrane of Fig. 4a is initially flat and free of any pretension, the tangent stiffness matrix is singular at the first

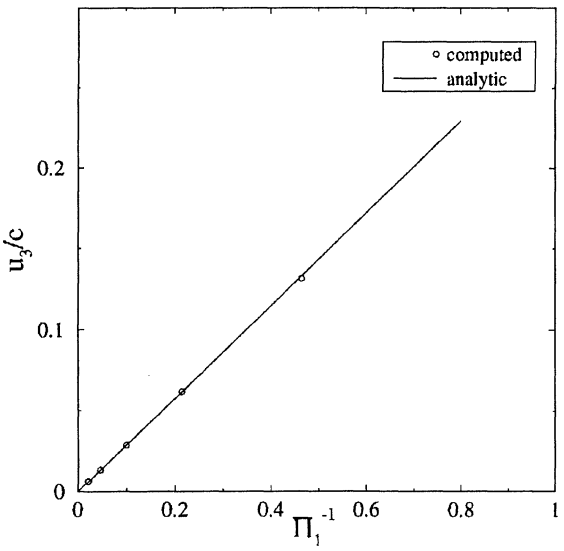

a) Midpoint displacement of a square, initially flat, edge constrained membrane subjected to uniform pressure load

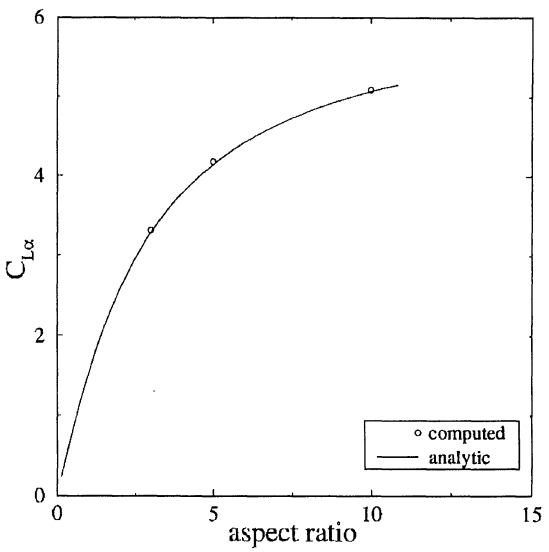

b) Lift curve slope for a rigid elliptical planform flat plate

Fig. 4 Numerical solutions computed using 256 quadrilateral elements.

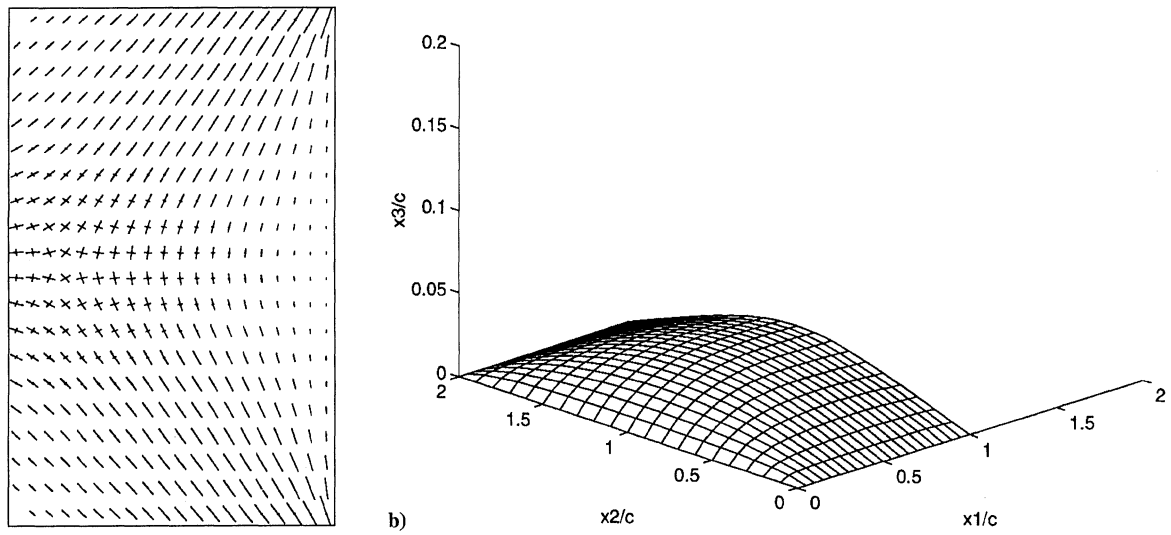

Fig. 5 Principal stresses and equilibrium configuration for a rectangular membrane wing with a free trailing edge; $\Pi_1 = 15$, $\alpha = 15$ deg, and $\nu = 0.5$.

load step and the load-stepping procedure immediately fails. Consequently, the solution strategy adopted for the test case of Fig. 4a was to prestrain the membrane for the first load step in order to remove the singularity and begin the load-stepping procedure, then subsequently remove the prestrain before assembling the tangent stiffness at the next load step. This prestraining strategy was also used for all aeroelastic cases that follow.

The accuracy of the lifting surface model may be tested by computing the lift curve slope C_{L_α} for a rigid elliptic planform flat plate of varying aspect ratio. A comparison is shown in Fig. 4b for three different aspect ratios. The agreement with the analytic result[21] can be seen to be quite good.

B. Application to Membrane Wings

The first aeroelastic case to be solved is that of an initially flat rectangular membrane wing of aspect ratio 2 shown in Fig. 5. The membrane is restrained all around the perimeter (${}^t u_i = 0,\ i = 1, 2, 3$) except for the trailing edge, which is free to deflect. The aeroelastic parameter Π_1 is 15, the angle of attack is 15 deg, and Poisson's ratio is 0.5. As can be seen in Fig. 5a, the stress state in the membrane is predominantly uniaxial with slack conditions being reported by several Gauss points at the corners near the leading edge. In Fig. 5a, the length of the line segments are proportional to the principal stresses and oriented in the same direction, and in Fig. 5b the wing coordinates are nondimensionalized by the wing chord c.

The chordwise aerodynamic loading for the rectangular membrane is shown in Fig. 6a with the convergence path of the explicit/implicit velocity-stepping algorithm shown in Fig. 6b. For this problem, the freestream velocity was increased incrementally taking 200 velocity steps to reach the value of Π_1 stated earlier. Only at the last velocity step was the Newton–Raphson procedure allowed to converge the solution to machine accuracy. By following this explicit/implicit strategy and taking a relatively large number of explicit steps before the Newton–Raphson iteration is allowed to begin, the explicitly computed approximate solution is essentially guaranteed to be within the convergence radius of the method without the need for an accurate a priori estimate of the equilibrium configuration. This strategy has proven to be effective in enhancing the stability and utility of the algorithm.

The second configuration to be investigated is that of an initially flat triangular planform marine sail of aspect ratio 4 in an unbounded fluid domain (no free surface or image sail), which is pinned at the leading edge (${}^t u_i = 0,\ i = 1, 3$) and at the clew (${}^t u_i = 0,\ i = 1, 2, 3$) with the foot and trailing edge free to deflect, as shown in Fig. 7. To more closely approximate the boundary conditions at the mast of the Marconi-rigged marine sail, the displacement degree of freedom parallel to the leading edge (${}^t u_2$) is free, and the membrane is allowed to slide along the leading-edge support. The aeroelastic parameter Π_1 is 17, the angle of attack is 20 deg, and Poisson's ratio is 0.5.

In Fig. 7b it can be seen that the initially flat sail develops camber and twists in response to the aerodynamic load. The stress field shown in Fig. 7a is almost entirely uniaxial with the tension at the head and clew becoming quite large in comparison to the rest of the sail. In a real sail the stress in these high-tension areas is kept in check by increasing the number of layers of sail cloth as required to maintain an acceptable stress level. The twist and camber developed in the sail can also be seen in the membrane cross sections, shown in Fig. 8b.

The computed chordwise aerodynamic loading for the sail configuration is shown in Fig. 8a. Although the aerodynamic loading decreases monotonically toward the trailing edge (the original constant strain, triangular membrane wing element proposed by Jackson and Christie[2] would typically give oscillatory aerodynamic loading profiles), the present formulation appears to have some difficulty at this level of discretization (576 elements) in implicitly satisfying the Kutta condition at midspan for this configuration. This difficulty at the trailing edge may be due to the wake geometry being fixed and restricted from assuming a natural force-free configuration or, perhaps more likely, it may be due to an inadequate discretization near the trailing edge. An improved element arrangement, e.g., a cosine spacing, would probably lead to a more accurate solution near the trailing edge. Similarly, a wake alignment procedure could easily be incorporated in the present algorithm; however, because the basic assumption of potential flow results in a fairly weak description of the actual fluid mechanics for sail configurations, the issue of wake alignment is probably of little consequence. The Marconi-rig sail problem described has been computationally investigated by others with essentially identical results to those presented here.[23]

Finally, the effect of grid refinement for the sail configuration is presented in Table 1. The induced drag shows the greatest dependency on grid resolution inasmuch as it is proportional to the square of the lift and is sensitive to the fidelity with which the wake is resolved. However, the integrated coefficients typically vary by only a few percent and are fairly insensitive to the discretization. In a related issue, the present implementation of the algorithm uses lower–upper decomposition[22] to solve the linear system of equations associated with both the elastic and aerodynamic problems. This method of solution becomes prohibitively inefficient for discretizations involving 500 elements or more. For discretization involving a larger number of unknowns, a more efficient linear solver is required. It has also been observed that underrelaxation, when

Table 1 Effect of grid refinement on the computed aerodynamic coefficients for an initially flat, Marconi-rigged marine sail configuration; $\Pi_1 = 17$, $\alpha = 20$ deg, and $\nu = 0.5$

Number of elements	$C_{M\,le}$	C_L	C_D
100	−0.171	1.08	0.0426
256	−0.168	1.06	0.0411
576	−0.166	1.05	0.0402

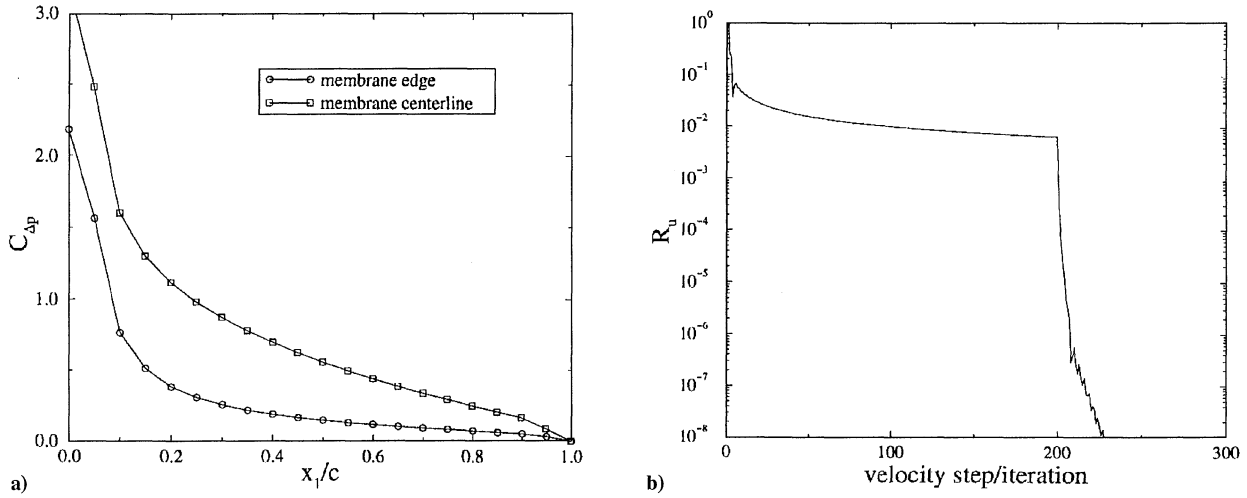

Fig. 6 Chordwise loading profiles and convergence path for the rectangular membrane wing with a free trailing edge; $\Pi_1 = 15$, $\alpha = 15$ deg, and $\nu = 0.5$.

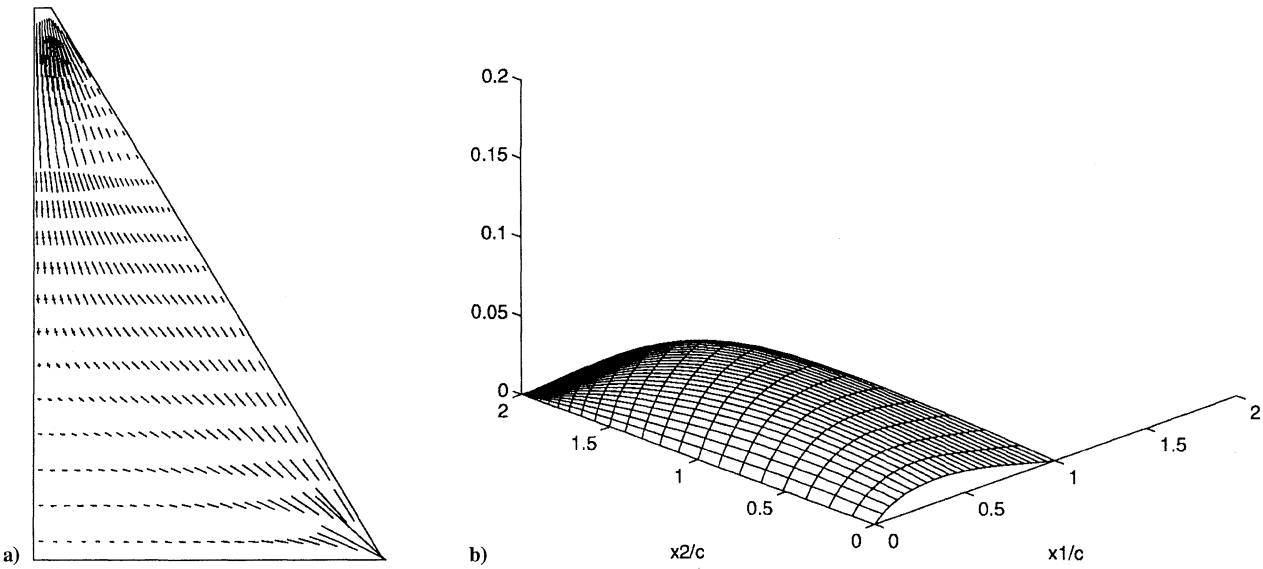

Fig. 7 Principal stresses and equilibrium configuration for a Marconi-rigged marine sail configuration; $\Pi_1 = 17$, $\alpha = 20$ deg, and $\nu = 0.5$.

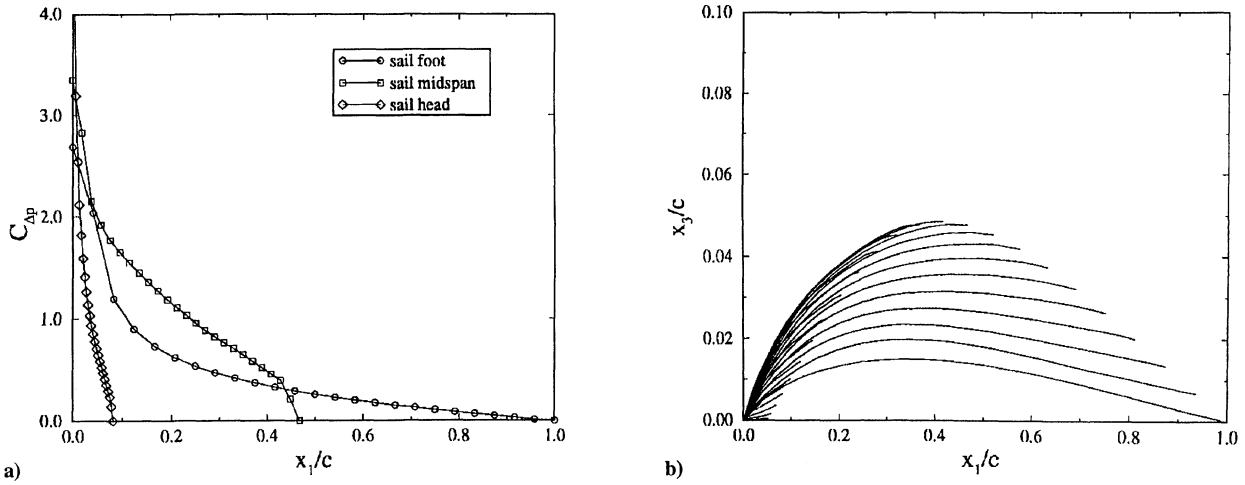

Fig. 8 Chordwise loading and equilibrium membrane profiles for a Marconi-rigged marine sail configuration; $\Pi_1 = 17$, $\alpha = 20$ deg, and $\nu = 0.5$.

applied to the incremental displacements in Eq. (2c), can significantly extend the range of parameters and configurations for which aeroelastic solutions can be obtained.

IV. Summary

The membrane wing element technology and associated algorithm presented here have been shown to satisfy two limiting cases of the aeroelastic problem where analytic solutions are available. In addition, the quadrilateral element was shown to satisfy monotonicity in chordwise loading for flexible membrane wings. Consequently, the present element technology may be considered a refinement of the constant strain triangular element technology originally proposed by Jackson and Christie.[2] Although the assumption of potential flow seriously restricts the range of applicability of the method, it offers a practical alternative to a high Reynolds number three-dimensional Navier–Stokes calculation for investigating membrane wing mechanics.

Appendix: Element Matrices

The element coordinates, displacements, and displacement increments are interpolated from their nodal values in the element coordinate system as follows:

$$\begin{bmatrix} x_1 \\ x_2 \\ x_3 \end{bmatrix} = [H]\begin{bmatrix} X_1^1 & X_2^1 & X_3^1 & X_1^2 & \cdots & X_3^4 \end{bmatrix}^T \tag{A1a}$$

$$\begin{bmatrix} {}^tu_1 \\ {}^tu_2 \\ {}^tu_3 \end{bmatrix} = [H]\begin{bmatrix} {}^tU_1^1 & {}^tU_2^1 & {}^tU_3^1 & {}^tU_1^2 & \cdots & {}^tU_3^4 \end{bmatrix}^T \tag{A1b}$$

$$\begin{bmatrix} u_1 \\ u_2 \\ u_3 \end{bmatrix} = [H]\begin{bmatrix} U_1^1 & U_2^1 & U_3^1 & U_1^2 & \cdots & U_3^4 \end{bmatrix}^T \tag{A1c}$$

where

$$[H] = \begin{bmatrix} h_1 & 0 & 0 & h_2 & 0 & 0 & h_3 & 0 & 0 & h_4 & 0 & 0 \\ 0 & h_1 & 0 & 0 & h_2 & 0 & 0 & h_3 & 0 & 0 & h_4 & 0 \\ 0 & 0 & h_1 & 0 & 0 & h_2 & 0 & 0 & h_3 & 0 & 0 & h_4 \end{bmatrix} \tag{A1d}$$

with the isoparametric interpolation functions h_1, h_2, h_3, and h_4 given as

$$h_1 = \tfrac{1}{4}(1-r)(1-s) \tag{A1e}$$

$$h_2 = \tfrac{1}{4}(1+r)(1-s) \tag{A1f}$$

$$h_3 = \tfrac{1}{4}(1+r)(1+s) \tag{A1g}$$

$$h_4 = \tfrac{1}{4}(1-r)(1+s) \tag{A1h}$$

where r and s are natural coordinates defined on the biunit square. The overbar indicating the local coordinate system shown in Fig. 2 has been dropped for convenience.

The element stiffness, force, and load matrices appearing in Eq. (6) are defined as follows:

$$[{}^tK_L] = \int_{0_V} [{}^tB_L]^T [C][{}^tB_L]\, {}^0\mathrm{d}V \tag{A2a}$$

$$[{}^tK_{\mathrm{NL}}] = \int_{0_V} [{}^tB_{\mathrm{NL}}]^T [{}^tS][{}^tB_{\mathrm{NL}}]\, {}^0\mathrm{d}V \tag{A2b}$$

$$[{}^{t+\Delta t}\boldsymbol{F}] = \int_{0_V} [{}^{t+\Delta t}B_L]^T [{}^{t+\Delta t}\hat{S}]\, {}^0\mathrm{d}V \tag{A2c}$$

$$[{}^{t+\Delta t}\boldsymbol{R}] = \int_{0_S} [H]^T [{}^{t+\Delta t}\boldsymbol{f}]\, {}^0\mathrm{d}S \tag{A2d}$$

Assuming a state of plane stress to exist in the element leads to the following choices for the stress state matrices:

$$[{}^tS] = \begin{bmatrix} {}^tS_{11} & {}^tS_{12} & 0 & 0 & 0 & 0 \\ {}^tS_{12} & {}^tS_{22} & 0 & 0 & 0 & 0 \\ 0 & 0 & {}^tS_{11} & {}^tS_{12} & 0 & 0 \\ 0 & 0 & {}^tS_{12} & {}^tS_{22} & 0 & 0 \\ 0 & 0 & 0 & 0 & {}^tS_{11} & {}^tS_{12} \\ 0 & 0 & 0 & 0 & {}^tS_{12} & {}^tS_{22} \end{bmatrix} \tag{A3a}$$

and

$$[{}^{t+\Delta t}\hat{S}] = \begin{bmatrix} {}^{t+\Delta t}S_{11} \\ {}^{t+\Delta t}S_{22} \\ {}^{t+\Delta t}S_{12} \end{bmatrix} \tag{A3b}$$

The linear strain transformation matrix is given by

$$[{}^tB_L] = [{}^tB_{L0}] + [{}^tB_{L1}] \tag{A4a}$$

where

$$[{}^tB_{L0}] = \begin{bmatrix} \dfrac{\partial h_1}{\partial x_1} & 0 & 0 & \dfrac{\partial h_2}{\partial x_1} & \cdots & 0 \\ 0 & \dfrac{\partial h_1}{\partial x_2} & 0 & 0 & \cdots & 0 \\ \dfrac{\partial h_1}{\partial x_2} & \dfrac{\partial h_1}{\partial x_1} & 0 & \dfrac{\partial h_2}{\partial x_2} & \cdots & 0 \end{bmatrix} \tag{A4b}$$

and

$$[{}^tB_{L1}] = \begin{bmatrix} l_{11}\dfrac{\partial h_1}{\partial x_1} & l_{21}\dfrac{\partial h_1}{\partial x_1} & l_{31}\dfrac{\partial h_1}{\partial x_1} & \cdot & l_{31}\dfrac{\partial h_4}{\partial x_1} \\ l_{12}\dfrac{\partial h_1}{\partial x_2} & l_{22}\dfrac{\partial h_1}{\partial x_2} & l_{32}\dfrac{\partial h_1}{\partial x_2} & \cdot & l_{32}\dfrac{\partial h_4}{\partial x_2} \\ l_{11}\dfrac{\partial h_1}{\partial x_2} + l_{12}\dfrac{\partial h_1}{\partial x_1} & l_{21}\dfrac{\partial h_1}{\partial x_2} + l_{22}\dfrac{\partial h_1}{\partial x_1} & l_{31}\dfrac{\partial h_1}{\partial x_2} + l_{32}\dfrac{\partial h_1}{\partial x_1} & \cdot & l_{31}\dfrac{\partial h_4}{\partial x_2} + l_{32}\dfrac{\partial h_4}{\partial x_1} \end{bmatrix} \tag{A4c}$$

with

$$l_{ij} = \left(\frac{\partial h_k}{\partial x_j}\right) {}^tU_i^k \qquad i, j = 1, 2, 3 \qquad \text{and} \qquad k = 1, 2, 3, 4 \tag{A4d}$$

Similarly, the nonlinear strain transformation matrix is given by

$$[{}^tB_{\mathrm{NL}}] = \begin{bmatrix} \dfrac{\partial h_1}{\partial x_1} & 0 & 0 & \dfrac{\partial h_2}{\partial x_1} & 0 & 0 & \dfrac{\partial h_3}{\partial x_1} & 0 & 0 & \dfrac{\partial h_4}{\partial x_1} & 0 & 0 \\ \dfrac{\partial h_1}{\partial x_2} & 0 & 0 & \dfrac{\partial h_2}{\partial x_2} & 0 & 0 & \dfrac{\partial h_3}{\partial x_2} & 0 & 0 & \dfrac{\partial h_4}{\partial x_2} & 0 & 0 \\ 0 & \dfrac{\partial h_1}{\partial x_1} & 0 & 0 & \dfrac{\partial h_2}{\partial x_1} & 0 & 0 & \dfrac{\partial h_3}{\partial x_1} & 0 & 0 & \dfrac{\partial h_4}{\partial x_1} & 0 \\ 0 & \dfrac{\partial h_1}{\partial x_2} & 0 & 0 & \dfrac{\partial h_2}{\partial x_2} & 0 & 0 & \dfrac{\partial h_3}{\partial x_2} & 0 & 0 & \dfrac{\partial h_4}{\partial x_2} & 0 \\ 0 & 0 & \dfrac{\partial h_1}{\partial x_1} & 0 & 0 & \dfrac{\partial h_2}{\partial x_1} & 0 & 0 & \dfrac{\partial h_3}{\partial x_1} & 0 & 0 & \dfrac{\partial h_4}{\partial x_1} \\ 0 & 0 & \dfrac{\partial h_1}{\partial x_2} & 0 & 0 & \dfrac{\partial h_2}{\partial x_2} & 0 & 0 & \dfrac{\partial h_3}{\partial x_2} & 0 & 0 & \dfrac{\partial h_4}{\partial x_2} \end{bmatrix} \tag{A4e}$$

Because the elastic membrane element will be used in conjunction with an inviscid flow model, the surface traction vector is taken to be normal to the element and equal to the pressure difference Δp across the membrane. This pressure difference is assumed to be uniform over each element. Consequently, the surface traction vector is given by

$$[{}^{t+\Delta t}f] = \begin{bmatrix} 0 \\ 0 \\ \Delta p \end{bmatrix} = \begin{bmatrix} 0 \\ 0 \\ p^- - p^+ \end{bmatrix} \tag{A4f}$$

where p^+ and p^- are the aerodynamic surface pressures on the upper and lower membrane surfaces, respectively.

The transformation relating the derivatives in physical coordinates to the derivatives in isoparametric coordinates is given by the chain rule. This transformation is

$$\begin{bmatrix} \dfrac{\partial}{\partial x_1} \\ \dfrac{\partial}{\partial x_2} \end{bmatrix} = \left(\frac{1}{J}\right) \begin{bmatrix} \dfrac{\partial x_2}{\partial s} & -\dfrac{\partial x_2}{\partial r} \\ -\dfrac{\partial x_1}{\partial s} & \dfrac{\partial x_1}{\partial r} \end{bmatrix} \begin{bmatrix} \dfrac{\partial}{\partial r} \\ \dfrac{\partial}{\partial s} \end{bmatrix} \tag{A5a}$$

where

$$J = \frac{\partial x_1}{\partial r}\frac{\partial x_2}{\partial s} - \frac{\partial x_1}{\partial s}\frac{\partial x_2}{\partial r} \tag{A5b}$$

The volume integrals appearing in Eqs. (A2a–A2d) are evaluated using 3×3 Gauss quadrature on the biunit square according to

$$\int_{0_V} (\,)^0 \mathrm{d}V = \mathrm{d}\int_{-1}^{+1}\int_{-1}^{+1} J(\,)\,\mathrm{d}r\,\mathrm{d}s \tag{A5c}$$

where d is the thickness of the element.

References

[1]Jackson, P. S., "The Analysis of Three-Dimensional Sails," *Proceedings of CANCAM*, Univ. of Western Ontario, Canada, 1985, pp. 59–67.

[2]Jackson, P. S., and Christie, G. W., "Numerical Analysis of Three-Dimensional Elastic Membrane Wings," *AIAA Journal*, Vol. 25, 1987, pp. 676–682.

[3]Miller, R. K., and Hedgepeth, J. M., "An Algorithm for Finite Element Analysis of Partly Wrinkled Membranes," *AIAA Journal*, Vol. 20, 1982, pp. 1761–1763.

[4]Nielsen, J. N., "Theory of Flexible Aerodynamic Surfaces," *Journal of Applied Mechanics*, Vol. 30, 1963, pp. 435–442.

[5]Sneyd, A. D., "Aerodynamic Coefficients and Longitudinal Stability of Sail Airfoils," *Journal of Fluid Mechanics*, Vol. 149, 1984, pp. 127–146.

[6]Ormiston, R. A., "Theoretical and Experimental Aerodynamics of the Sailwing," *Journal of Aircraft*, Vol. 8, 1971, pp. 77–81.

[7]Murai, H., and Maruyama, S., "Theoretical Investigation of the Aerodynamics Sailwing Airfoils Taking Account of Elasticities," *Journal of Aircraft*, Vol. 19, 1982, pp. 385–389.

[8]Holla, V. S., Rao, K. P., Asthana, C. B., and Arokkiaswamy, A., "Aerodynamic Characteristics of Pretensioned Elastic Membrane Rectangular Sailwings," *Computer Methods in Applied Mechanics and Engineering*, Vol. 44, 1984, pp. 1–16.

[9]Kroo, I., "Aeroelasticity in Very Light Aircraft," *Recent Trends in Aeroelasticity*, edited by P. Hajela, Univ. of Florida Press, Gainesville, FL, 1986, pp. 315–321.

[10]Thwaites, B., "Aerodynamic Theory of Sails," *Proceedings of the Royal Society of London*, Vol. 261, 1961, pp. 402–442.

[11]Smith, R. W., and Shyy, W., "Computation of Unsteady Laminar Flow over a Flexible Two-Dimensional Membrane Wing," *Physics of Fluids*, Vol. 7, 1995, pp. 2175–2184.

[12]Smith, R. W., and Shyy, W., "Computation of Aerodynamic Coefficients for a Flexible Membrane Airfoil in Turbulent Flow: A Comparison with Classical Theory," *Physics of Fluids*, Vol. 8, 1996, pp. 3346–3353.

[13]Newman, B. G., "Aerodynamic Theory for Membranes and Sails," *Progress in Aerospace Sciences*, Vol. 24, 1987, pp. 1–27.

[14]Bathe, K. J., *Finite Element Procedures in Engineering Analysis*, Prentice–Hall, Englewood Cliffs, NJ, 1984, pp. 301–379.

[15]Malvern, L. E., *Introduction to the Mechanics of a Continuous Medium*, Prentice–Hall, Englewood Cliffs, NJ, 1969, pp. 31, 32.

[16]Stein, M., and Hedgepeth, J. M., "Analysis of Partly Wrinkled Membranes," NASA TN D-813, 1961.

[17]Miller, R. K., Hedgepeth, J. M., Weingarten, V. I., Das, P., and Kahyai, S., "Finite Element Analysis of Partly Wrinkled Membranes," *Computers and Structures*, Vol. 20, 1985, pp. 631–639.

[18]James, R. M., "On the Remarkable Accuracy of the Vortex Lattice Method," *Computer Methods in Applied Mechanics and Engineering*, Vol. 1, 1972, pp. 55–79.

[19]Katz, J., and Plotkin, A., *Low Speed Aerodynamics*, McGraw–Hill, New York, 1991, pp. 378–386.

[20]Seide, P., "Large Deflections of Rectangular Membranes Under Uniform Pressure," *International Journal of Nonlinear Mechanics*, Vol. 12, 1977, pp. 397–406.

[21]Van Dyke, M., *Perturbation Methods in Fluid Mechanics*, Parabolic, Stanford, CA, 1975, pp. 239, 240.

[22]Press, W. H., Teukolsky, S. A., Vetterling, W. T., and Flannery, B. P., *Numerical Recipes*, Cambridge Univ. Press, Cambridge, England, UK, 1992.

[23]Johnston, M. S., "An Aeroelastic Model for the Analysis of Membrane Wings and its Application to the Flight of Pteranondon Ingens," Ph.D. Thesis, Dept. of Mechanical Engineering, Univ. of Auckland, New Zealand, 1997.

A. Plotkin
Associate Editor